Electronic and nuclear contributions in sub-GeV dark matter scattering:
A case study with hydrogen

Jiunn-Wei Chen,[1,2,3] Hsin-Chang Chi,[4] C.-P. Liu,[4,*] Chih-Liang Wu,[1,†] and Chih-Pan Wu[1]

[1]*Department of Physics, National Taiwan University, Taipei 10617, Taiwan*
[2]*Center for Theoretical Sciences and Leung Center for Cosmology and Particle Astrophysics,*
National Taiwan University, Taipei 10617, Taiwan
[3]*Helmholtz-Institut für Strahlen- und Kernphysik and Bethe Center for Theoretical Physics,*
Universität Bonn, D-53115 Bonn, Germany
[4]*Department of Physics, National Dong Hwa University, Shoufeng, Hualien 97401, Taiwan*
(Received 17 August 2015; published 30 November 2015)

The scattering of sub-GeV dark matter (DM) particles with hydrogen atoms is studied in this paper. The interactions of DM with electrons and nucleons are both included and formulated in a general framework based on nonrelativistic effective field theory. On the assumption of the same dark matter coupling strengths, it is found that DM-electron interactions dominate the inelastic atomic transitions to discrete excited states and ionization continuum around the threshold regions, and DM-nucleon interactions become more important with increasing energy and dominate in elastic scattering. The conclusion should apply, qualitatively, to practical detector species so that electronic and nuclear contributions in DM scattering processes can be disentangled, while issues including binding effects and the recoil mechanism in many-body systems will require further detailed calculations.

I. INTRODUCTION

The existence of dark matter (DM) has been concretely established based on gravitational evidence from various scales of the Universe. However, its composition and non-gravitational interactions, if any, are still unknown. Among all DM candidates, the weakly interacting massive particles (WIMPs) receive the most attention mainly because of the so-called WIMP miracle: with a DM particle mass $m_\chi \sim$ 10 GeV–1 TeV and a self-annihilation cross section similar to the one of the weak interaction, WIMPs can explain the relic DM abundance of the Universe. By looking for the nuclear recoil triggered by WIMP scattering in detectors, null results of direct searches have ruled out quite a bit of WIMP parameter space (for the current status, see, e.g., [1] and the references therein), and future multiton experiments will further improve the limit (or produce a discovery).

On the other hand, the dark sector consisting of light DM (LDM) particles with masses below 10 GeV has also attracted interest recently (for an overview, see, e.g., [2] and the references therein). First of all, there is no reason to exclude such possibilities *a priori*, and, in fact, many well-motivated models predict their existence: for example, WIMP-less [3,4] and asymmetric DM with m_χ varying between MeV and GeV scales, several proposals at MeV ranges [5–10], and keV ranges including bosonic super-WIMP [11], axinos [12–14], and sterile neutrinos [15–19].

Furthermore, in order to accommodate low-energy anomalies in astrophysical sources such as the 511 keV [20,21] (reviewed in [22]) and 3.5 keV [23,24] emission lines, and the GeV γ-ray excesses in the Galactic center [25,26], LDM candidates are often proposed as possible answers.

As most of these LDM candidates do not have sufficient energy to produce detectable nuclear recoils in present-day (and near-future) detectors, direct searches for them have to rely on electron recoils. Therefore, unlike typical WIMP searches which set limits on DM-nucleon interactions, they can be used to constrain DM-electron interactions by either DM-impact ionization [27,28] or dark photoionization [29]. One particularly interesting case is the interpretation of the potential light WIMP signal ($m_\chi \sim$ 10 GeV, which is at the mass upper end of LDM) reported by the DAMA/LIBRA experiment [30–32]. To reconcile its tension with other stringent constraints set by direct experiments on WIMP-nucleon interactions, models of DM that are leptophilic but not hadrophilic provide viable solutions (see, e.g., [33–35]). In addition to direct searches of LDM and/or its interactions with electrons, alternative searches through indirect signals and colliders are also reported [36–38].

If DM interacts both with electrons and nucleons, an important question naturally arises: In a specific DM scattering process which a direct search detector is built to look for, what are the contributions from the electronic and nuclear degrees of freedom? Even though the current common practice in constraining DM interactions is one type at a time, it is necessary to keep in mind that events measured by a detector are a sum from all possible sources. Furthermore, it is desirable from the experimental point of view to determine which

*Corresponding author.
cpliu@mail.ndhu.edu.tw
†Present address: Center for Theoretical Physics, Massachusetts Institute of Technology, Cambridge, MA 02139, USA.

process and kinematic region would be best to constrain a certain type of DM interactions with electrons or nucleons. For this purpose, one has to rely on theoretical analysis.

In this article, we try to address the above questions using the simplest atom, hydrogen—where most calculations can be carried out analytically—and study its scattering with nonrelativistic LDM particles of a MeV-GeV mass range. As the associated energy and momentum transfer of such scattering processes overlap with typical atomic scales, one expects that atomic physics plays an important role and that issues like binding effects and electron/nuclear recoils require detailed study. The simplistic setup of hydrogen should therefore result in a useful qualitative understanding which applies to more intricate systems.

The paper is organized as follows. In Sec. II, the general formalism is developed for scattering channels, including elastic, discrete excitation, and ionization ones. The DM-electron and DM-nucleon interactions are formulated in a general way based on effective field theory (EFT). In addition to commonly discussed spin-independent and spin-dependent contact interactions, which are the leading-order terms in the EFT expansion, we also include the possibility of long-range DM interactions (for example, through the kinetic mixing of dark and normal photons) and a few next-to-leading-order terms. In Sec. III, we present and discuss our results, and we make inferences from these generic features that will apply to other atoms including those practically being used in mainstream DM detectors. Finally, a summary is in Sec. IV.

II. FORMALISM

Direct searches of DM look for signals as results of DM scattering off normal matter. As the nature of DM and its nongravitational interactions with normal matter are still unknown, instead of considering specific, well-motivated models, we adopt a general approach based on EFT. A nonrelativistic (NR) EFT that accommodates scalar, fermionic, and vector DM particles with velocity $v_\chi \ll 1$[1] and their interactions with protons (p) and neutrons (n) via intermediate scalar and vector bosons is formulated in Ref. [39], and it is fully worked out to next-to-next-to-leading order in Ref. [40]. In this work, we further take electrons into account and focus on the kinematic region where electrons also behave like NR particles.

At leading order (LO), the effective interaction takes the form

$$L_{\text{int}}^{(\text{LO})} = \sum_{f=e,p,n} \left\{ c_1^{(f)} (\chi^\dagger \chi)(f^\dagger f) + c_4^{(f)} (\chi^\dagger \vec{S}_\chi \chi) \cdot (f^\dagger \vec{S}_f f) \right.$$
$$\left. + d_1^{(f)} \frac{1}{q^2} (\chi^\dagger \chi)(f^\dagger f) + d_4^{(f)} \frac{1}{q^2} (\chi^\dagger \vec{S}_\chi \chi) \cdot (f^\dagger \vec{S}_f f) \right\},$$
$$(1)$$

---

where χ and f denote the NR DM and fermion fields, respectively, $\vec{S}_{\chi,f}$ are their spin operators (scalar DM particles have null $\vec{S}_\chi$), the magnitude of the DM 3-momentum transfer $q = |\vec{q}|$ depends on the DM energy transfer T and its scattering angle θ. Note that we use the same nomenclature as in [40] for the low-energy constant (LEC) $c_i^{(f)}$'s that characterize the types of the χ-f contact interactions. Correspondingly, the LEC $d_i^{(f)}$'s are used to describe potential $U(1)$-like, long-range χ-f interactions that are results of, e.g., mixing of dark and ordinary photons via $\epsilon F'_{\mu\nu} F^{\mu\nu}$, where $F'_{\mu\nu}$ and $F_{\mu\nu}$ refer to the field tensors of the dark and ordinary photons, respectively, and ϵ the mixing angle. These LECs correspond to the ones in [39] by $c_1 \to h_1$, $c_4 \to h_2$, $d_1 \to l_1$, and $d_4 \to l_2$.

To simplify the presentation of the full scattering formula for an unpolarized DM scattering off a hydrogen atom, we start with the simplified case where only one of the LECs is assumed to be nonzero. (Note: This is the conventional practice in DM searches.) Following the standard scattering theory (for more details, see, e.g., Ref. [41]), the differential cross section in the laboratory frame for DM being scattered solely by the $c_1^{(e)}$ term in Eq. (1) into the final 3-momentum $\vec{k}_2$ with an infinitesimal phase volume $d^3 k_2$ is expressed by

$$d\sigma|_{c_1^{(e)}} = \frac{2\pi}{v_\chi} \sum_F \overline{\sum_I} |\langle F|c_1^{(e)} e^{i\frac{\mu}{m_e}\vec{q}\cdot\vec{r}}|I\rangle|^2$$
$$\times \delta(T - E_{\text{c.m.}} - (E_F - E_I)) \frac{d^3 k_2}{(2\pi)^3}. \quad (2)$$

The reduced mass $\mu = m_e m_p / (m_e + m_p)$ with $m_{e(p)}$ being the mass of the electron (proton); for later use, the mass of hydrogen is designated $M_{\text{H}} = M - B$, with $M = m_e + m_p$ and B being the binding energy. The initial state $|I\rangle$ denotes the hydrogen atom at the ground state, i.e., the spatial part $|I\rangle_{\text{spatial}} = |1s\rangle$. The Dirac delta function imposes the energy conservation that the energy deposited by DM equals to the recoil energy of the atomic center of mass, $E_{\text{c.m.}}$, plus the internal excitation energy $E_F - E_I$ of the atom.

Depending on the nature of the final state $\langle F|$, the scattering processes are classified as

(1) elastic scattering (el): $_{\text{spatial}}\langle F| = \langle 1s|$; $E_{\text{c.m.}} = q^2/(2M_{\text{H}})$ and $E_F - E_I = 0$,

(2) discrete excitation (ex): $_{\text{spatial}}\langle F| = \langle nlm_l|$, with $(n, l, m_l) \neq (1, 0, 0)$; $E_{\text{c.m.}} = q^2/(2M_{\text{H}})$ and $E_F - E_I = E_{nl} - E_{1s}$,

(3) ionization (ion): $_{\text{spatial}}\langle F| = \langle \vec{p}_r|$, with $\vec{p}_r$ denoting the relative momentum in the c.m. frame; $E_{\text{c.m.}} = q^2/(2M)$ and $E_F - E_I = B + p_r^2/(2\mu)$.

The symbol $\overline{\sum}_I$ represents an average over the initial magnetic (and spin, when spin operators are involved)

states; $\sum_F$ means a sum over all the final magnetic and spin (and spin, too) states for elastic scattering and discrete excitation, while for ionization, the sum over magnetic states is replaced by $\int d^3\vec{p}_r/(2\pi)^3$.

Given the analytic forms of wave functions

$$\langle 100|\vec{r}\rangle = \frac{1}{\sqrt{\pi}} Z^{\frac{3}{2}} e^{-Z\bar{r}}, \tag{3}$$

$$\langle nlm_l|\vec{r}\rangle = \frac{1}{(2l+1)!} \sqrt{\frac{(n+l)!}{2n(n-l-1)!}} \left(\frac{2Z}{n}\right)^{\frac{3}{2}} e^{-\frac{Z\bar{r}}{n}} \left(\frac{2Z\bar{r}}{n}\right)^l {}_1F_1\left(-(n-l-1), 2l+2, \frac{2Z\bar{r}}{n}\right) Y_l^{m_l*}(\theta, \phi), \tag{4}$$

$$\langle \vec{p}_r|\vec{r}\rangle = e^{\frac{\pi Z}{2\bar{p}_r}} \Gamma\left(1 - \frac{iZ}{\bar{p}_r}\right) e^{-i\vec{p}_r\cdot\vec{r}} {}_1F_1\left(\frac{iZ}{\bar{p}_r}, 1, i(p_r r + \vec{p}_r\cdot\vec{r})\right) \tag{5}$$

in atomic units [so that barred quantities $\bar{r} = rm_e\alpha$ and $\bar{p}_r = p_r/(m_e\alpha)$], where $\Gamma(z)$ and ${}_1F_1(a, b, z)$ are the gamma and confluent hypergeometric functions, respectively, we can calculate all of the transition matrix elements analytically by the Nordsieck integration techniques [42–45]. The response function relevant for transitions to discrete states is found to be

$$R^{(nl)}(\kappa) = \sum_{m_l} |\langle nlm_l|e^{i\vec{\kappa}\cdot\vec{r}}|1s\rangle|^2$$

$$= (2l+1)\mathcal{I}_{nl}^2, \tag{6}$$

$$\mathcal{I}_{nl}(\kappa) = \frac{(-1)^{n-l-1}}{4n^2(2l+1)!} \sqrt{\frac{\pi(n+l)!}{(n-l-1)!} \frac{\Gamma(2l+2)}{\Gamma(n+l+1)} \frac{\Gamma(2l+3)}{\Gamma(l+3/2)}} \left(\frac{\bar{\kappa}}{4Z}\right)^l$$

$$\times \left(\frac{d}{dt}\right)^{n-l-1} \left[(1-t)^{n+l+1}\left((1-t)^2 + \left(\frac{\bar{\kappa}}{2Z}\right)^2\right)^{-l-2}\right]\Bigg|_{t=0}, \tag{7}$$

which is dimensionless. The response function relevant for transitions to continuum is

$$R^{(\text{ion})}(\kappa) = \int d^3p_r |\langle \vec{p}_r|e^{i\vec{\kappa}\cdot\vec{r}}|1s\rangle|^2 \delta\left(T - B - \frac{\vec{q}^2}{2M} - \frac{\vec{p}_r^2}{2\mu}\right)$$

$$= \frac{2^8 Z^6 \bar{q}^2 (3\bar{\kappa}^2 + \bar{p}_r^2 + Z^2) \exp\left[-\frac{2Z}{\bar{p}_r}\tan^{-1}\left(\frac{2Z\bar{p}_r}{\bar{\kappa}^2 - \bar{p}_r^2 + Z^2}\right)\right]}{3m_e\alpha^2((\bar{\kappa} + \bar{p}_r)^2 + Z^2)^3((\bar{\kappa} - \bar{p}_r)^2 + Z^2)^3(1 - \exp^{\frac{-2\pi Z}{\bar{p}_r}})}\Bigg|_{p_r=\sqrt{2\mu(T-B-\frac{\bar{q}^2}{2M})}}, \tag{8}$$

where the factor of $m_e\alpha^2$ in the denominator gives the dimension as the energy conserving delta function is included in the definition.

Using the generic response functions obtained above, the single differential cross section with respect to energy transfer, $d\sigma/dT$, can be compactly expressed. For elastic scattering or discrete excitation to the final discrete level (nl),

$$\frac{d\sigma^{(nl)}}{dT}\Bigg|_{c_1^{(e)}} = \frac{1}{2\pi} \frac{m_H}{v_\chi^2} |c_1^{(e)}|^2 R^{(nl)}\left(\kappa = \frac{\mu}{m_e} q\right), \tag{9}$$

$$\text{with} \quad q^2 = 2M_H(T - (E_{nl} - E_{1s})). \tag{10}$$

The $1/v_\chi^2$ factor in Eq. (9) comes from two sources, with each one contributing $1/v_\chi$: (i) division by flux in $d\sigma/dT$ and (ii) the integration of the DM scattering angle $\cos\theta$ with respect to the energy conserving delta function. Note that it does not lead to physical singularity when taking an extremely NR limit $v_\chi \to 0$ since the DM flux and the kinetic energy both approach zero. The magnitude of q is determined by energy conservation or, equivalently, the scattering angle $\cos\theta$ is fixed once the energy transfer T for such two-to-two-body scattering is known. For ionization processes

$$\frac{d\sigma^{(\text{ion})}}{dT}\Bigg|_{c_1^{(e)}} = \frac{1}{2\pi} \frac{m_\chi}{v_\chi} k_2 \int d\cos\theta |c_1^{(e)}|^2 R^{(\text{ion})}\left(\kappa = \frac{\mu}{m_e} q\right), \tag{11}$$

with $\min\left\{1, \max\left[-1, \dfrac{k_1^2 + k_2^2 - 2M(T-B)}{2k_1 k_2}\right]\right\}$

$$\leq \cos\theta \leq 1, \tag{12}$$

where $k_1 = m_\chi v_\chi$ and $k_2 = (m_\chi^2 v_\chi^2 - 2m_\chi T)^{1/2}$ are the magnitudes of the initial and the final momentum, respectively. Because the final atomic state has two bodies to share the transferred energy and momentum, the DM scattering angle $\cos\theta$ now can span a finite range for a given energy transfer T.

Next we consider the $d_1^{(e)}$ term. Because its Lagrangian differs from $c_1^{(e)}$ term only by a kinematic factor $1/q^2$ (which only causes a rescaling of transition matrix elements), it can easily be calculated by replacing $c_1^{(e)}$ to $d_1^{(e)}/q^2$ in both Eq. (9) and Eq. (11). If both terms exist, then one has to take their coherent interference into account, so that the coupling in front of the response functions becomes $c_1^{(e)} + d_1^{(e)}/q^2$.

Unlike the $c_1^{(e)}$ and $d_1^{(e)}$ terms, which are independent of the spins of the DM and the scattered particles, the $c_4^{(e)}$ and $d_4^{(e)}$ terms give rise to what are typically called spin-dependent interactions. Their matrix elements for unpolarized scattering involve additionally the initial spin average and the final spin sum. For a spinor with spin quantum number s and m_s, it yields

$$\sum_{m_s'} \overline{\sum_{m_s}} \langle s, m_s'|S_a|s, m_s\rangle \langle s, m_s'|S_b|s, m_s\rangle^* = \frac{1}{3}s(s+1)\delta_{ab}. \tag{13}$$

With the DM spin s_χ and the electron spin $s_e = 1/2$, the spin averages and sums applied to both the DM and electron parts yield a product: $s_\chi(s_\chi + 1)/4$. Other than this factor, the rest of the spatial matrix elements are completely the same as in the $c_1^{(e)}$ and $d_1^{(e)}$ case. As a result, the corresponding scattering formula can be obtained by changing $|c_1^{(e)} + d_1^{(e)}/q^2|^2$ to $\frac{1}{4}s_\chi(s_\chi + 1)|c_4^{(e)} + d_4^{(e)}/q^2|^2$ in both Eq. (9) and Eq. (11).

It is worthwhile to point out here that there is no interference between the spin-independent interactions with c_1, d_1 and the spin-dependent one with c_4, d_4, in unpolarized scattering, since the trace of a spin matrix is zero.

Now we consider the cases where DM scatters off the proton instead of the electron. Besides the trivial change of LECs, the most important difference is due to the fact that the proton is much closer to the atomic center of mass than the electron. After factoring out the center-of-mass motion, the resulting atomic transition operators in its intrinsic frame are

$$\rho^{(e)}(\vec{q}) = e^{i\frac{\mu}{m_e}\vec{q}\cdot\vec{r}}, \tag{14}$$

$$\rho^{(p)}(\vec{q}) = e^{-i\frac{\mu}{m_p}\vec{q}\cdot\vec{r}}, \tag{15}$$

for the electron and the proton, respectively. This leads to the following change of the corresponding response functions:

$$R_e^{(nl,\mathrm{ion})} = R^{(nl,\mathrm{ion})}\left(\kappa = \frac{\mu}{m_e}q\right), \tag{16}$$

$$R_p^{(nl,\mathrm{ion})} = R^{(nl,\mathrm{ion})}\left(\kappa = \frac{\mu}{m_p}q\right), \tag{17}$$

and similarly in the differential cross section formulas, Eqs. (9) and (11).

Finally, we can summarize the above derivation and obtain the differential cross section formulas for DM scattering off the hydrogen atom at LO. For transitions to discrete states,

$$\left.\frac{d\sigma^{(nl)}}{dT}\right|_{\mathrm{LO}} = \frac{1}{2\pi}\frac{m_\mathrm{H}}{v_\chi^2}\left\{\sum_{f=e,p}\left(\left|c_1^{(f)} + \frac{d_1^{(f)}}{q^2}\right|^2 + \frac{1}{4}s_\chi(s_\chi + 1)\left|c_4^{(f)} + \frac{d_4^{(f)}}{q^2}\right|^2\right)R_f^{(nl)} \right.$$
$$\left. + 2(c_1^{(e)} + d_1^{(e)}/q^2)(c_1^{(p)} + d_1^{(p)}/q^2)^* R_{ep}^{(nl)}\right\}\Bigg|_{q^2 = 2M_\mathrm{H}(T - (E_{nl} - E_{1s}))}, \tag{18}$$

and for ionizations,

$$\left.\frac{d\sigma^{(\mathrm{ion})}}{dT}\right|_{\mathrm{LO}} = \frac{1}{2\pi}\frac{m_\chi}{v_\chi}k_2\int d\cos\theta\left\{\sum_{f=e,p}\left(\left|c_1^{(f)} + \frac{d_1^{(f)}}{q^2}\right|^2 + \frac{1}{4}s_\chi(s_\chi + 1)\left|c_4^{(f)} + \frac{d_4^{(f)}}{q^2}\right|^2\right)R_f^{(\mathrm{ion})} \right.$$
$$\left. + 2(c_1^{(e)} + d_1^{(e)}/q^2)(c_1^{(p)} + d_1^{(p)}/q^2)^* R_{ep}^{(\mathrm{ion})}\right\}\Bigg|_{p_r^2 = 2\mu(T - B - q^2/(2M))}. \tag{19}$$

In these formulas, there are two new response functions $R_{ep}^{(nl,\mathrm{ion})}$ defined which describe the nontrivial interference between the spin-independent χ-e and χ-p amplitudes; they are

$$R_{ep}^{(nl)} = \sqrt{R_e^{(nl)} R_p^{(nl)}} \tag{20}$$

and

$$R_{ep}^{(\text{ion})} = \int d^3 p_r \langle \vec{p}_r | e^{i\frac{\mu}{m_e}\vec{q}\cdot\vec{r}} | 1s \rangle \langle \vec{p}_r | e^{-i\frac{\mu}{m_p}\vec{q}\cdot\vec{r}} | 1s \rangle^* \delta\left(T - B - \frac{\vec{q}^2}{2M} - \frac{\vec{p}_r^2}{2\mu}\right). \tag{21}$$

Note that there is no interference between the $c_4^{(e)}$ and $c_4^{(p)}$ terms, nor between the $d_4^{(e)}$ and $d_4^{(p)}$ terms, as they involve different spin operators, with each of them traceless.

Even though we mainly concentrate on the LO interaction with DM in this article, we shall also consider a few terms at next-to-leading order (NLO):

$$\begin{aligned}
L_{\text{int}}^{(\text{NLO})} = \sum_{f=e,p,n} \Big\{ &c_{10}^{(f)} (\chi^\dagger \chi)(f^\dagger i\vec{\sigma}_f \cdot \vec{q}f) + c_{11}^{(f)} (\chi^\dagger i\vec{\sigma}_\chi \cdot \vec{q}\chi)(f^\dagger f) \\
&+ d_{10}^{(f)} \frac{1}{q^2} (\chi^\dagger \chi)(f^\dagger i\vec{\sigma}_f \cdot \vec{q}f) + d_{11}^{(f)} \frac{1}{q^2} (\chi^\dagger i\vec{\sigma}_\chi \cdot \vec{q}\chi)(f^\dagger f) \Big\} + \cdots.
\end{aligned} \tag{22}$$

They translate into the ones of [39] by $c_{11} \to h_1'$, $c_{10} \to h_2'$, $d_{11} \to l_1'$, and $d_{10} \to l_2'$. Because the spin operators that come with the $c_{11}^{(e,p)}$ and $c_{10}^{(e,p)}$ terms are mutually independent (after spin average and sum) with each other except for the interference between $c_{11}^{(e)}$ and $c_{11}^{(p)}$, and also with all LO terms, including them in Eqs. (18) and (19) is straightforward by

$$\left(\left| c_1^{(f)} + \frac{d_1^{(f)}}{q^2} \right|^2 + \frac{1}{4} s_\chi(s_\chi + 1) \left| c_4^{(f)} + \frac{d_4^{(f)}}{q^2} \right|^2 \right)$$

$$\to \left(\left| c_1^{(f)} + \frac{d_1^{(f)}}{q^2} \right|^2 + \frac{1}{4} s_\chi(s_\chi + 1) \left| c_4^{(f)} + \frac{d_4^{(f)}}{q^2} \right|^2 + \frac{1}{3} s_\chi(s_\chi + 1) q^2 \left| c_{11}^{(f)} + \frac{d_{11}^{(f)}}{q^2} \right|^2 + \frac{1}{4} q^2 \left| c_{10}^{(f)} + \frac{d_{10}^{(f)}}{q^2} \right|^2 \right)$$

$$(c_1^{(e)} + d_1^{(e)}/q^2)(c_1^{(p)} + d_1^{(p)}/q^2)^*$$

$$\to (c_1^{(e)} + d_1^{(e)}/q^2)(c_1^{(p)} + d_1^{(p)}/q^2)^* + \frac{1}{3} s_\chi(s_\chi + 1) q^2 (c_{11}^{(e)} + d_{11}^{(e)}/q^2)(c_{11}^{(p)} + d_{11}^{(p)}/q^2)^*, \tag{23}$$

where a similar argument is applied to the $d_{11}^{(e,p)}$ and $d_{10}^{(e,p)}$ terms.

III. RESULTS AND DISCUSSIONS

In this section, we give numerical results for two different DM masses: (i) $m_\chi = 1$ GeV and (ii) $m_\chi = 50$ MeV, and both with a nonrelativistic velocity $v_\chi = 10^{-3}$. While our formalism works for any DM masses, the chosen cases sample one high-mass candidate close to the LDM mass upper edge, and one low-mass candidate which has enough kinetic energy to ionize a hydrogen atom.[2] (Decreasing m_χ further will first close the ionization channel, then the discrete excitations, and will eventually leave only elastic scattering.) Our main purpose is to illustrate and discuss how the electron and the proton, respectively, contribute to the scattering processes for specified EFT interaction terms and reaction channels. For clarity of presentation, we ignore all interference terms and assume the DM interaction strengths with the electron and the proton are the same when making comparisons between the electronic and nuclear contributions. It should be borne in mind that the total cross section is a sum of all contributions from the electron and the proton with interference terms included.

A. LO interactions of c_1, d_1, c_4, and d_4

The upper two panels of Fig. 1 show the differential cross sections $d\sigma/dT$ for DM scattering with $m_\chi = 1$ GeV and the c_1-type interactions. For the nuclear part (the right panel), the elastic scattering dominates all of the other channels by orders of magnitude. The reason is obvious: Since the momentum scale that determines the nuclear response $\kappa_p = \mu/m_p q \sim \mu/m_p m_\chi v_\chi \sim 0.5$ keV is smaller than the inverse of the atomic size, $m_e \alpha \sim 3$ keV, it is a

---

[2]Note that we only consider DM scattering in this work. For cases such as a dark photon γ' that can be kinetically mixed to a real photon, then a dark photoabsorption with $m_{\gamma'} > 13.6$ eV can induce hydrogen ionization.
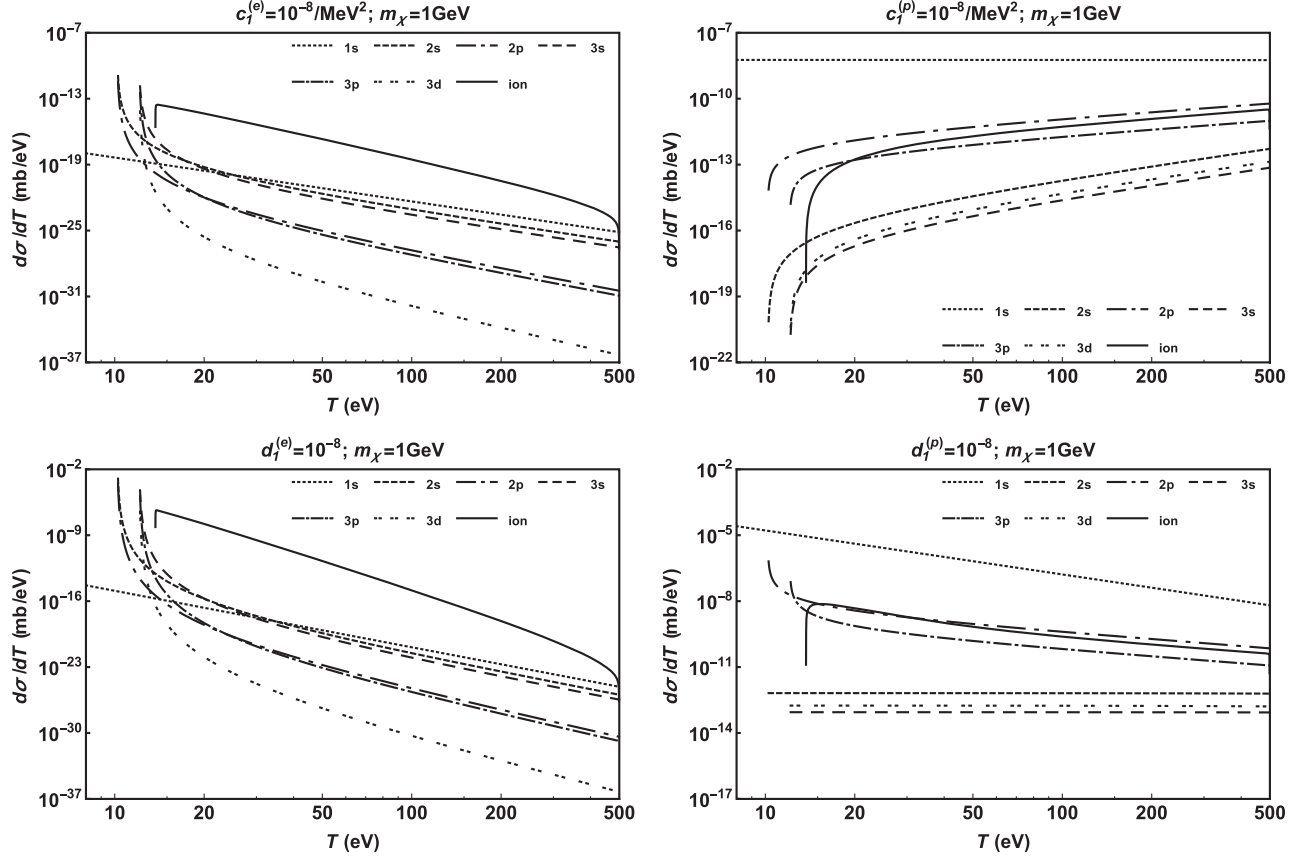
FIG. 1. Different channels of DM scattering with $m_\chi = 1$ GeV and interaction of $c_1^{(e)} = 10^{-8}/\text{MeV}^2$ (upper-left panel), $c_1^{(p)} = 10^{-8}/\text{MeV}^2$ (upper-right panel), $d_1^{(e)} = 10^{-8}$ (lower-left panel), $d_1^{(p)} = 10^{-8}$ (lower-right panel).

good approximation that the nuclear charge operator can be expanded as $\rho(\vec{\kappa}_p) \sim 1 - i\vec{\kappa}_p \cdot \vec{r} + \cdots$. Unlike the elastic scattering, all of the inelastic channels have no leading-order contributions because of wave function orthogonality. Also, because the next-to-leading-order operator is a dipole operator, the excitations to the final p-orbitals or continuum are more probable than other discrete states. For the electronic part (the left panel), the results change dramatically. First, as the momentum scale that determines the electronic response $\kappa_e = \mu/m_e q \sim \mu/m_e m_\chi v_\chi \sim 1$ MeV is much bigger than the inverse of the atomic size, the electric charge operator $\rho(\vec{\kappa}_e) = e^{i\vec{\kappa}_e \cdot \vec{r}}$ becomes highly oscillating. As a result, the elastic differential cross section shows the familiar form factor suppression. On the other hand, in discrete excitations, one does observe much larger cross sections in near-threshold regions. The reason is most of the energy transferred T by DM is given to internal excitation; this leaves the 3-momentum transfer $q = \sqrt{2M_H(T - (E_{nl} - E_{1s}))}$ becoming quite small, so that the form factor suppression is less severe. Among all reaction channels arising from the $c_1^{(e)}$-type interaction, the ionization channel is the dominant one in most of the kinematic region, for it can access more of the kinematic phase space with small q. In addition, the peaks near

discrete excitation thresholds also provide good observation windows for not only the large cross section but also the clean signal of deexcitation photons of definite energies.

In the lower two panels of Fig. 1, the results for the d_1-type interactions are shown. The numerical changes from the previous c_1-type results are mainly due to adding a $1/q^2$ factor to the scattering amplitude (or a $1/q^4$ one to the double differential cross section). Because $q^2 = 2m_H T$ in elastic scattering, this leads to an extra $1/T^2$ dependence in $d\sigma/dT$ and can best be illustrated by observing the difference of the (almost) flat line and the power-law-decreasing line in the $c_1^{(p)}$ and $d_1^{(p)}$ plots, respectively. For discrete excitation channels, except for the near-threshold region, one expects a similar $1/T^2$ dependence when T gets bigger than the excitation energies. The case of the ionization channel is more intricate, as q^2 is to be integrated over a range allowed by kinematics; there is no simple scaling from the c_1- to d_1-type results. Overall, the long-range interaction yields sharper energy dependence of $d\sigma/dT$ than the contact one for all of the scattering channels considered. The elastic scattering is still the best channel to constrain $d_1^{(p)}$, and discrete excitations at thresholds and ionization the best for $d_1^{(e)}$.

In Fig. 2, similar plots—but with $m_\chi = 50$ MeV—are shown. The most noticeable differences from Fig. 1 are (i) the NR DM kinetic energy is smaller, so $T_{max} = \frac{1}{2}m_\chi v_\chi^2 = 25$ eV and (ii) in elastic scattering and discrete excitations, the maximum allowed energy transfers are cut off at smaller values: 4.8, 14.0, and 15.7 eV for final $n = 1$, 2, 3 states, respectively. The latter is due to maintaining energy and momentum conservation in the final two-body system (the DM particle and the atom) with $m_\chi \leq M_H$. Using Eq. (10) and setting the maximum DM scattering angle $\cos\theta = -1$, one can get an approximate formula

$$T_{cut}^{(nl)} = \frac{4m_\chi M_H}{(m_\chi + M_H)^2} T_{max} + \frac{M_H - m_\chi}{M_H + m_\chi}(E_{nl} - E_{1s}), \quad (24)$$

which yields the correct cutoff energies that were just pointed out, except that the cutoffs in energy transfer, the $d\sigma/dT$'s of the elastic scattering and the discrete excitations are the same for both $m_\chi = 50$ MeV and $m_\chi = 1$ GeV in the allowed range of T. Because the associated response functions, which depend on the 3-momentum transfer q, are fixed by T and the excitation energy, the independence of m_χ is thus understood. Note that these cutoff energies limit

the ability of direct LDM searches because the recoil energies are too small to be detected.

On the other hand, $d\sigma/dT$ of the ionization channel shows different features. First, as there are three bodies in the final states (the DM particle, the ionized atom, and the ejected electron), energy and momentum conservation does not introduce a kinematic cutoff, so T can extend to the end point energy T_{max}. For this reason, the ionization channel should be considered as the golden mode to LDM direct searches. Second, the value of q does depend on m_χ, via Eq. (12); as a result, $d\sigma/dT$ is not m_χ independent. To make the comparison clear, the results of $m_\chi = 1$ GeV are plotted with the thin solid curves in the same figures.

At $T \approx 17$ eV, one observes discontinuities in $d\sigma/dT$ in the right panels of Fig. 2. This is the combined result of two ingredients. (i) The scattering angle is bounded by Eq. (12). At $T \approx 17$ eV, the maximum scattering angle 180° is reached [this energy can also be anticipated from Eq. (24) with the excitation energy $E_{nl} - E_{1s}$ being replaced by the binding energy $-E_{1s}$], so the integration range in Eq. (11) ceases to increase for $T > 17$ eV. (ii) The nuclear response function $R_p^{(ion)}$ is bigger at backward angles than forward angles, so the integral Eq. (11)
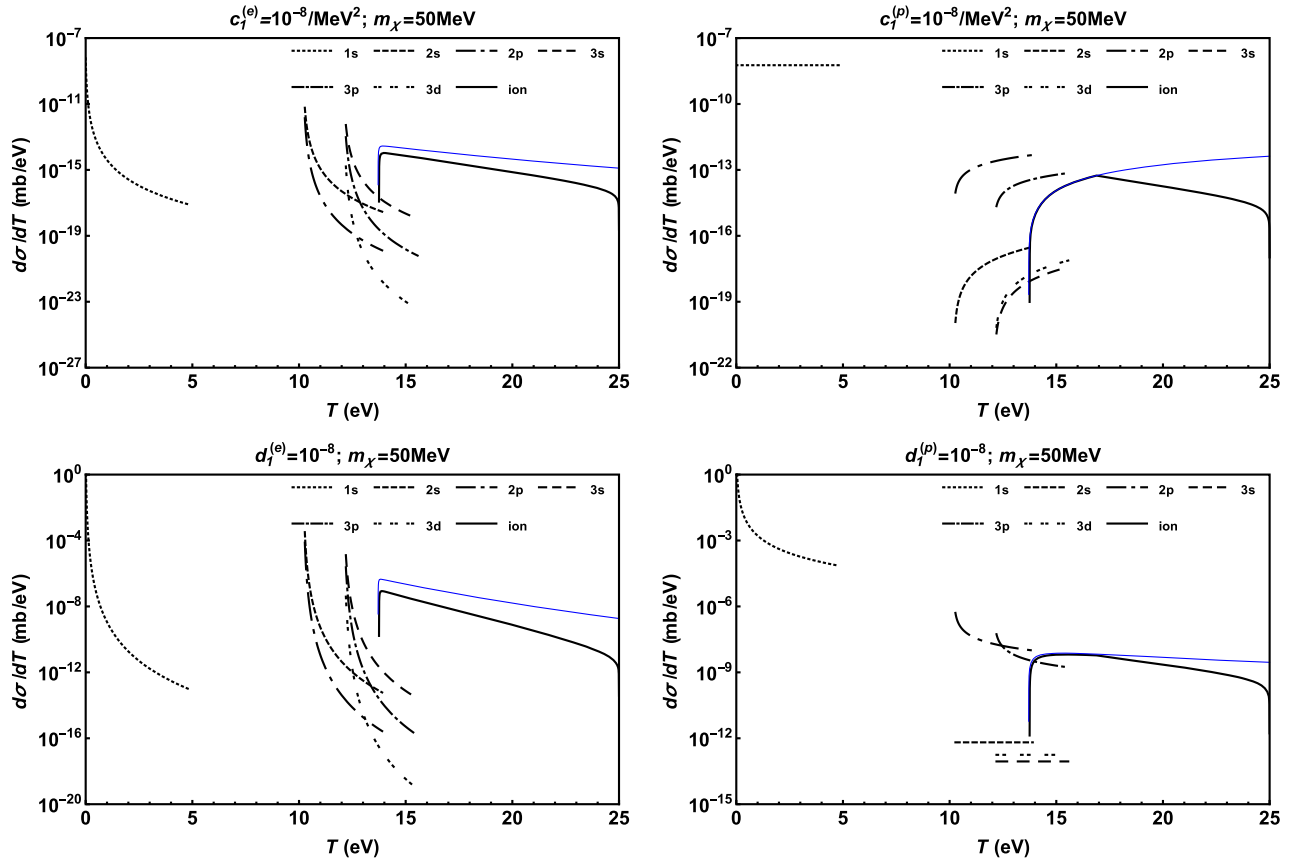

FIG. 2 (color online).   Different channels of DM scattering with $m_\chi = 50$ MeV and interaction of $c_1^{(e)} = 10^{-8}/\text{MeV}^2$ (upper-left panel), $c_1^{(p)} = 10^{-8}/\text{MeV}^2$ (upper-right panel), $d_1^{(e)} = 10^{-8}$ (lower-left panel), $d_1^{(p)} = 10^{-8}$ (lower-right panel). The thin blue curves are the ionization results with $m_\chi = 1$ GeV, shown for comparison. (Note: Unlike Fig. 1, these are linear-log plots.)

sensitively depends on the integration range and its discontinuity. On the contrary, the electronic response function $R_e^{(\text{ion})}$ is only significant at small angles; therefore, the discontinuity in the integration range of Eq. (11) does not yield observable results in the left panels of Fig. 2.

The hydrogen atom only has one electron and one nucleon, so the contributions from the c_4- and d_4-type interactions are related to the ones of the c_1- and d_1-type interactions simply by a rescaling of one-body spin matrix element, as was discussed in the last section. We shall not repeat these plots, but just note that for other atoms with more electrons and nucleons, the spin-dependent cross sections from interaction terms like c_4 and d_4 do not receive many-body enhancement compared with the spin-independent interactions terms like c_1 and d_1.

As DM interactions with electrons and nucleons are both included in our calculations, it is interesting to compare their contributions. Assuming the same coupling constants, $c_1^{(e)} = c_1^{(p)} = 10^{-8}/\text{MeV}^2$, $d_1^{(e)} = d_1^{(p)} = 10^{-8}$, the comparison shown in Fig. 3 reveals several important features:

(1) In elastic scattering, the nuclear contribution dominates and is bigger than the electronic part by several orders of magnitude. Therefore, elastic scattering is not likely to be a good channel of constraining the LO DM-electron interactions if the LO DM-nucleon interactions are present and not unnaturally suppressed.

(2) In discrete excitations, the nuclear and electronic contributions have sharp crossovers at energies slightly bigger than excitation energies. If a detector is able to resolve these peaks where electronic contributions clearly dominate, then it can be useful for setting more stringent limits on the LO DM-electron interactions.

(3) In ionization processes, unlike discrete excitations, the electronic contributions generally dominate over

the nuclear parts up to some T beyond the ionization thresholds. As a result, the LO DM-electron interactions can hopefully be constrained in broader kinematic regions.

In Fig. 4, we study the m_χ dependence of the crossover energy below which the DM-electron cross section begins to be bigger than the DM-proton one (assuming the same coupling strength) via the c_1- or d_1-type interaction that gives rise to hydrogen ionization. The first thing to notice is that, in both types of interactions and the considered range of m_χ (50 MeV to 5 GeV), there exist certain ranges of DM energy transfer T where the ionization processes are more sensitive to the DM-electron interaction than the DM-nucleon one. Furthermore, one observes that the crossover energy for the d_1-type interaction is larger than the one for the c_1-type interaction. The main reason is the $1/q^4$ factor appearing in the double differential cross section gives more weight to the response function at low q^2, which enhances the role of electrons on one hand and suppresses the role of nucleons on the other.

Therefore, it is reasonable to conclude that the best observational window to look for the LO DM-electron interactions is ionization processes near threshold, in particular for LDM with $m_\chi < M_H$. The discrete excitation peaks (which need good energy resolution of detectors) also provide good supplements. Although hydrogen can hardly be a good candidate for detecting LO DM-electron interactions for the low-energy transfer $T \sim 10\text{--}20$ eV is far below the current detector thresholds, our conclusion above makes good sense for practical detector species made of heavy atoms: Not only the ionization thresholds of atomic inner orbitals can be as high as a few or tens of keV which are observable in current detectors, but also there is more than one ionization peak which can provide additional information.

At this point, we briefly comment on our choice of the coupling constants to make plots in Figs. 1–4. For $c_1^{(e)}$, as it
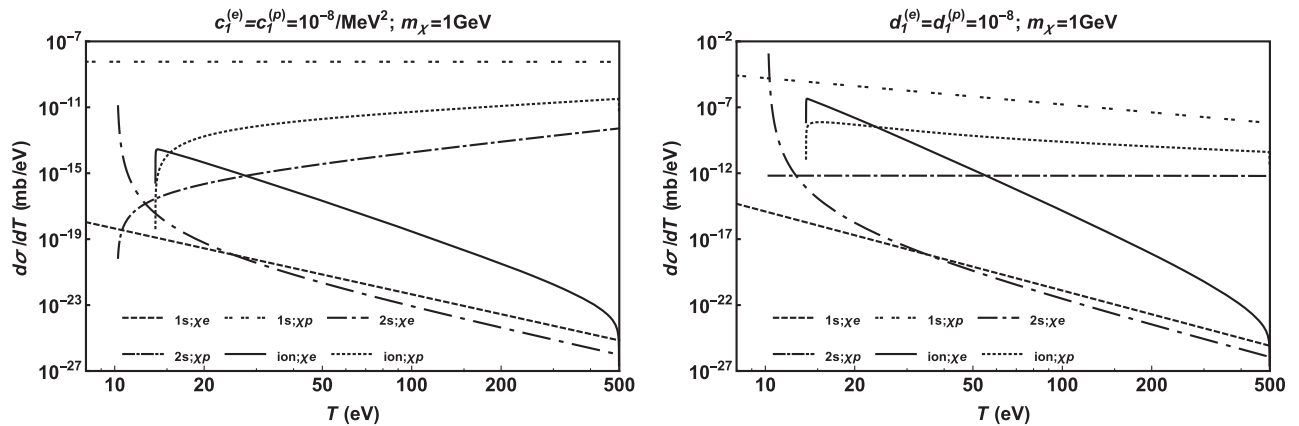

FIG. 3. Comparison of DM cross sections with the electron (χe) and proton (χp) in a hydrogen atom for selected channels including (i) elastic ($1s$), (ii) discrete excitation to $2s$, and (iii) ionization (ion). The interactions are taken to be (left panel) $c_1^{(e)} = c_1^{(p)} = 10^{-8}/\text{MeV}^2$ and (right panel) $d_1^{(e)} = d_1^{(p)} = 10^{-8}$. Interference terms due to χe and χp amplitudes are ignored.
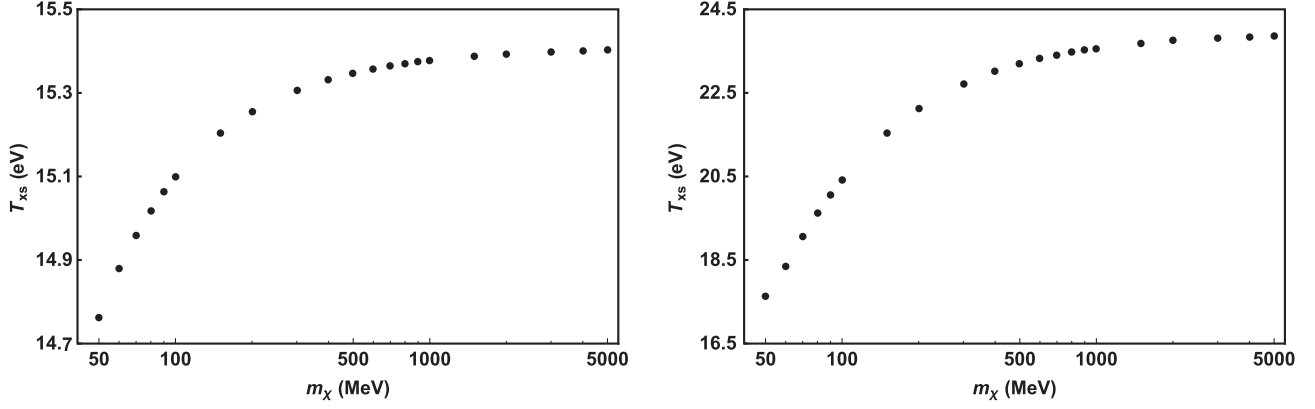
FIG. 4.   Energy transfer of DM, T_{xs}, below which scattering with the electron yields $d\sigma/dT$ bigger than the proton in the hydrogen ionization (assuming the same χe and χp coupling strengths), plotted against the DM mass m_χ for the c_1-type (left panel) and d_1-type (right panel) interaction terms.

can be related to the total cross section of LDM scattering off free electrons by

$$\sigma_e = \frac{1}{4\pi} m_e m_\chi |c_1^{(e)}|^2, \tag{25}$$

we choose $c_1^{(e)} = 10^{-8}/\text{MeV}^2$, using the upper limit recently set by XENON10 data [28]: $\sigma_e \lesssim 10^{-37}$ cm^2 for $m_\chi \sim 50$ MeV. For $d_1^{(e)}$, we simply assign a momentum scale $\Lambda \sim 1$ MeV and fix it to be $d_1^{(e)} = 10^{-8}$ so that $c_1^{(e)}$ and $d_1^{(e)}/\Lambda^2$ are comparable. As for $c_1^{(p)}$ and $d_1^{(p)}$, we make them the same as $c_1^{(e)}$ and $d_1^{(e)}$, respectively, to facilitate direct comparisons of the electron and nuclear contributions. Note that there are stringent limits set on $c_1^{(p)}$ and $d_1^{(p)}$ on the WIMP mass range 10 GeV $\lesssim m_\chi \lesssim 1$ GeV; however, they are largely unconstrained at LDM mass range in direct searches through nuclear recoils. Also, it is worth pointing out that there are complementary ways of constraining the LDM parameter space, for example, at $m_\chi \sim 50$ MeV, from the final state radiation of LDM annihilation $\chi + \bar{\chi} \to e^+ + e^-$, σ_e was claimed to be constrained at the 10^{-32}–10^{-33} cm^2 level [36],[3] and using the specific channel $e^+ + e^- \to \gamma + \chi + \bar{\chi}$ in electron-positron colliders, σ_e was reported reaching down to 10^{-42} cm^2 and can be further improved [37].[4]

B. NLO interactions of c_{11}, d_{11}, c_{10}, and d_{10}

Consider now the interaction terms of c_{11} and d_{11}, the results for $m_\chi = 1$ GeV are presented in Fig. 5. The main

---

[3]The paper reported a velocity-averaged cross section $\langle \sigma v \rangle$, we simply take $v = 10^{-3}$ here.
[4]The paper used a dark photon model, and the value extracted here corresponds to a dark photon mass of 3 GeV, which is considered to be heavy so that the interaction resembles the contact c_1 type we discuss.

change from the corresponding plots of c_1 and d_1 is the extra q^2 factor appearing in the differential cross sections. For elastic scattering or discrete excitations away from threshold, this factor introduces an extra dependence on T and again can be best seen by a comparison of the $c_1^{(p)}$ and $c_{11}^{(p)}$ curves for elastic scattering. For ionization, the impact of the q^2 factor, which is to be integrated over some allowed range, cannot, however, be easily factored out.

Our previous argument that the $d\sigma/dT$'s of elastic scattering and discrete excitations are independent of m_χ also applies to the cases of c_{11} and d_{11} (also c_{10} and d_{10}, to be discussed later). Therefore, we do not repeat the results for $m_\chi = 50$ MeV and just point out that they are the same as for the $m_\chi = 1$ GeV case in the regions bounded by the cutoff energies given by Eq. (24). Also, while the ionization processes do have m_χ dependence, it does not differ from what has been shown in Fig. 2 for the case of c_1 and d_1 in a significant way.

Similar to the c_1- and d_1-type interactions with DM, elastic scattering is the best to constrain the $c_{11}^{(p)}$ and $d_{11}^{(p)}$ terms, while inelastic scattering at discrete excitation peaks and of ionization are more suitable for the $c_{11}^{(e)}$ and $d_{11}^{(e)}$ terms. To further disentangle the dependence of $d\sigma/dT$ on c_1, d_1, c_{11}, and d_{11}, the scaling of $d\sigma/dT$ with energy transfer T can provide useful guidance: For example, in elastic scattering and discrete excitations away from thresholds, the energy dependence of $d\sigma/dT$ on the $|c_1|^2, |d_1|^2, |c_{11}|^2$, and $|d_{11}|^2$ terms is T^0, T^{-2}, T^1, and T^{-1}, respectively.

The pattern regarding the competition of electronic and nuclear contributions in discrete excitations and ionization with the c_{11} and d_{11} terms is similar to the case with the c_1 and d_1 terms: sharp crossovers in discrete excitations and some ranges of electronic dominance near the ionization threshold. Some examples are given in Fig. 6.

The energy transfer T_{xs} below which the electronic contribution is bigger than the nuclear one, assuming
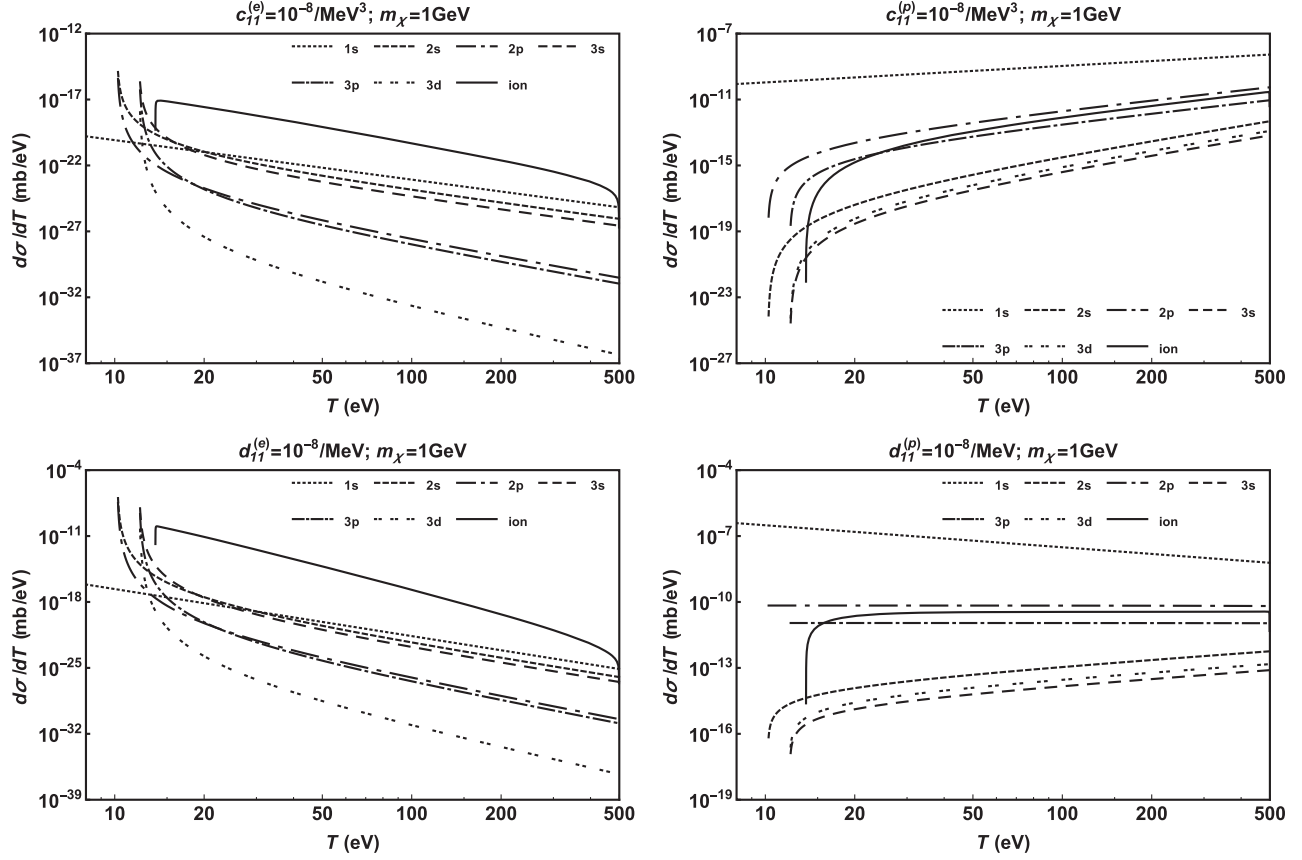
FIG. 5.   Different channels of DM scattering with $m_\chi = 1$ GeV and interaction of $c_{11}^{(e)} = 10^{-8}/\text{MeV}^3$ (upper-left panel), $c_{11}^{(p)} = 10^{-8}/\text{MeV}^3$ (upper-right panel), $d_{11}^{(e)} = 10^{-8}/\text{MeV}$ (lower-left panel), and $d_{11}^{(p)} = 10^{-8}/\text{MeV}$ (lower-right panel).

$c_{11}^{(e)} = c_{11}^{(p)} = 10^{-8}/\text{MeV}^3$ and $d_{11}^{(e)} = d_{11}^{(p)} = 10^{-8}/\text{MeV}$, in the ionization processes is plotted in Fig. 7 against m_χ. Notice that the values of T_{xs} for the c_{11}- and d_{11}-type interactions at a given m_χ are both reduced in comparison with the cases of the LO c_1 and d_1 terms, respectively. This is in agreement with the expectation that the extra q^2 factor

in the double differential cross section reduces the weight of the small q^2 region, so the electronic contribution is suppressed relative to the nuclear part.

Similar to the LO case, the contributions from the target-spin-dependent c_{10} and d_{10} terms can be obtained from the target-spin-independent results of c_{11} and d_{11}, simply by
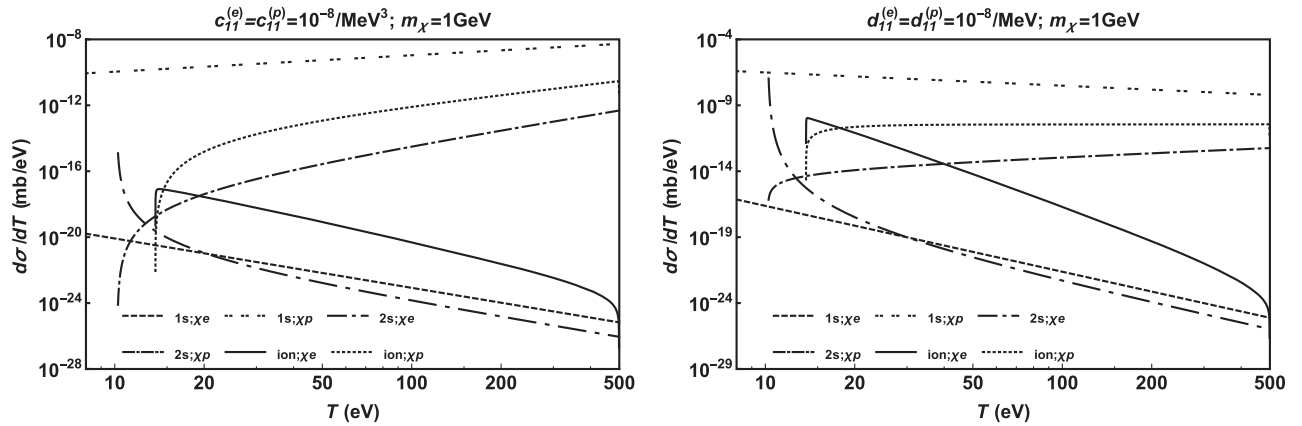

FIG. 6.   Comparison of DM cross sections with the electron (χe) and proton (χp) in a hydrogen atom for selected channels including (i) elastic (1s), (ii) discrete excitation to 2s, and (iii) ionization (ion). The interactions are taken to be $c_{11}^{(e)} = c_{11}^{(p)} = 10^{-8}/\text{MeV}^3$ (left panel) and $d_{11}^{(e)} = d_{11}^{(p)} = 10^{-8}/\text{MeV}$ (right panel). Interference terms resulting from χe and χp amplitudes are ignored.
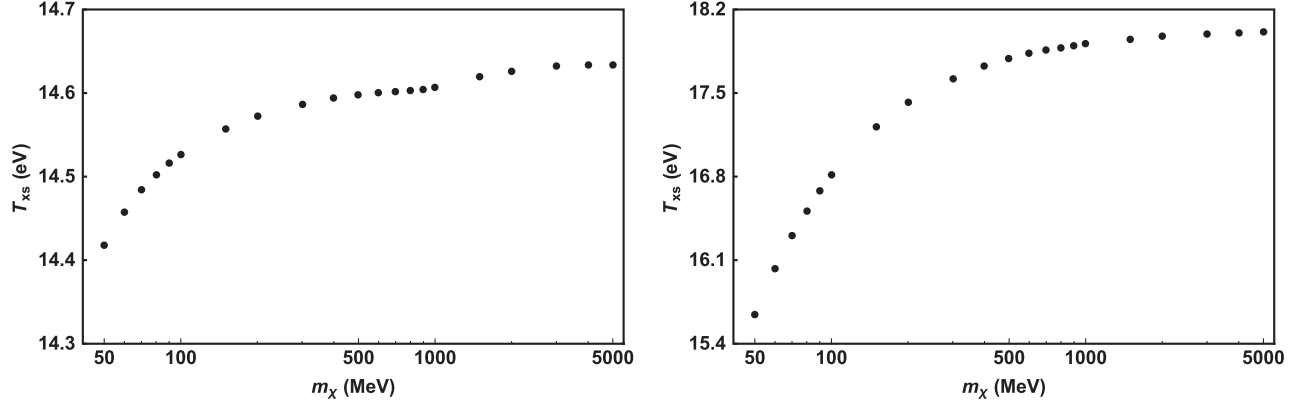
FIG. 7.   Energy transfer of DM, T_{xs}, below which scattering with an electron yield $d\sigma/dT$ bigger than the proton in the hydrogen ionization (assuming the same χe and χp coupling strengths), plotted against the DM mass m_χ for the c_{11}-type (left panel) and d_{11}-type (right panel) interaction terms.

adding factors resulting from spin matrix elements [see Eq. (13)]. Therefore, all observations and conclusions made in the c_{11} and d_{11} cases apply to the c_{10} and d_{10} ones.

However, regarding the competition between the electronic and nuclear contributions in scattering processes involving the c_{10} or d_{10} term, there is a subtlety arising from the natural scales of $c_{10}^{(e)}/c_{10}^{(p)}$ and $d_{10}^{(e)}/d_{10}^{(p)}$. If one

takes the point of view that EFT interaction terms of both electrons and nucleons are matched to a more fundamental theory at some high scale Λ, then it is reasonable to anticipate the possibility that $c_{10}^{(e)}/c_{10}^{(p)} \sim 1$ and $d_{10}^{(e)}/d_{10}^{(p)} \sim 1$. On the other hand, the masses of an electron and a nucleon differ by 3 orders of magnitude. If the c_{10} and d_{10} terms are matched to a relativistic theory, for example, $(\bar{\chi}\chi)(\bar{f}i\gamma_5 f)$
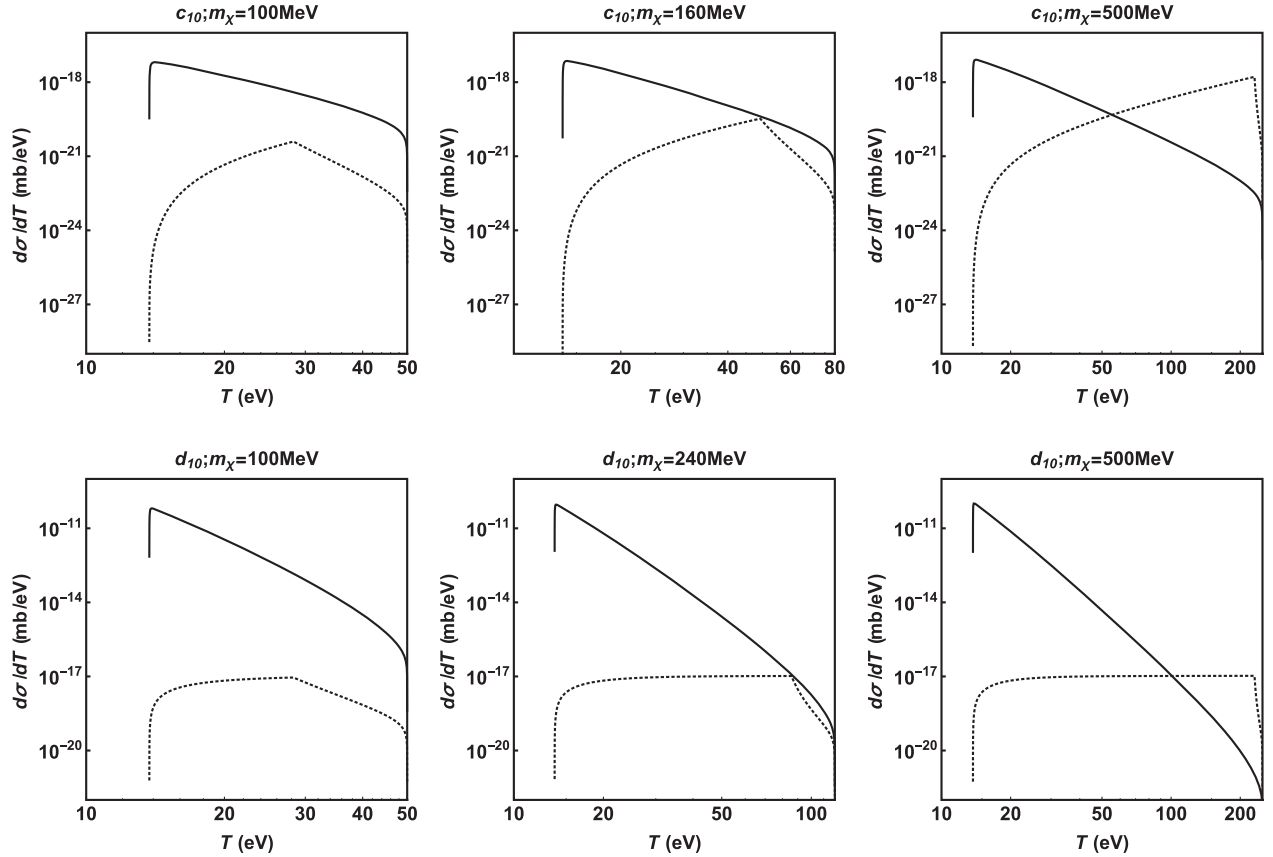

FIG. 8.   Comparison of electronic (solid lines) and nuclear (dotted lines) contributions to $d\sigma/dT$ for selected DM masses m_χ with $c_{10}^{(e)} = c_{10}^{(p)} m_p^2/m_e^2 = 10^{-8}/\mathrm{MeV}^3$ (upper panels) and $d_{10}^{(e)} = d_{10}^{(p)} m_p^2/m_e^2 = 10^{-8}/\mathrm{MeV}$ (lower panels).

and $(\bar{\chi}\chi)(\bar{f}i\gamma_5 f)/q_\mu^2$ at some high scale, the resulting nonrelativistic EFT expansion at NLO will involve the expansion parameter q/m_f to first order. In such cases, then one should expect $c_{10}^{(e)}/c_{10}^{(p)}, d_{10}^{(e)}/d_{10}^{(p)} \sim m_p/m_e \sim 2 \times 10^3$. This, in turn, would largely increase the sensitivity of discrete excitation peaks and ionization processes on the NLO DM-electron interaction terms such as c_{10} and d_{10}.

An example is given in Fig. 8: For $m_\chi \lesssim 160$ MeV and $m_\chi \lesssim 240$ MeV, respectively, for the c_{10} and d_{10} terms, the electronic contributions are larger than the nuclear ones in the entire allowed ranges of $T \leq \frac{1}{2}m_\chi v_\chi^2$. For heavier m_χ, the crossovers both happen at energies farther away from ionization thresholds, ~ 50 and 100 eV, respectively, for the c_{10} and d_{10} terms—much bigger than the other interaction terms previously discussed.

Briefly concluding this subsection, we point out that the best observational window to look for the NLO DM-electron interactions terms including c_{11}, d_{11}, c_{10}, and d_{10} is still the ionization processes near threshold and the discrete excitation peaks. The different energy dependence of $d\sigma/dT$ from the LO terms provides, in principle, a way to disentangle them. Furthermore, because of the huge difference between the masses of an electron and a nucleon, interaction terms that depend on the relativity of scattered particles can be further separated. In most situations, such NLO DM-electron interactions can be sensitively constrained without much background arising from similar DM-nucleon interactions because atomic electron can be very relativistic while atomic nuclei and nucleons inside are mostly nonrelativistic.

C. Background estimate

While hydrogen alone is not a practical detector species (although it indeed contributes in detectors which involve organic compounds), it is interesting to give a rough estimate of the possible backgrounds in our considered processes. Similar to WIMP direct searches, neutrino scattering is the most important one and is hardly reducible. As we discuss very low-energy transfer in scattering, in general below keV, the solar neutrinos from all reactions (electron type when produced) with peak energies spread around 100 keV to 10 MeV can contribute, and $E_\nu \gg T$ generally holds in our cases.

First, we give formulas for neutrino scattering off free fermions: For ν_e-e scattering (see, e.g., Ref. [46]),

$$\frac{d\sigma^{(\nu_e e)}}{dT} \approx \frac{G_F^2}{4\pi} m_e [(1 + 4\sin^2\theta_w)^2 + (-1)^2]$$

$$\sim 7.6 \times 10^{-24}\ \frac{\text{mb}}{\text{eV}}, \tag{26}$$

where $G_F \sim 10^{-5}/\text{GeV}^2$ is the Fermi constant and θ_w is the Weinberg angle with $\sin^2\theta_w \sim 0.238$ at low energies. For ν_μ-e and ν_τ-e scattering (appearing due to neutrino

oscillation), the only change (as there is only neutral current interaction) in formula is replacing the vector coupling $(1 + 4\sin^2\theta_w)$ into $(1 - 4\sin^2\theta_w)$ with the axial coupling (-1) unchanged. For ν_e-p scattering (see, e.g., Ref. [47,48]),

$$\frac{d\sigma^{(\nu_e p)}}{dT} \approx \frac{G_F^2}{4\pi} m_p [(1 - 4\sin^2\theta_w)^2 + g_A^2] \sim 4.7 \times 10^{-21}\ \frac{\text{mb}}{\text{eV}}, \tag{27}$$

where the vectors coupling $(1 - 4\sin^2\theta_w) \sim 0.05$ is usually defined as the proton weak charge $Q_w^{(p)}$, which is smaller than the neutron $Q_w^{(n)} = -1$ by one order of magnitude, and the axial coupling $g_A = 1.27$ is the nucleon axial charge. There is no change in formula for ν_μ-p and ν_τ-p since neutrino mass difference is totally negligible. Comparing Eqs. (26) and (27), one sees that ν-p scattering is more important than ν-e at low T roughly by the mass ratio $m_p/m_e \sim 10^3$.

For neutrino scattering off hydrogen, the binding effect has to be taken into account. The general differential cross section formulas can be derived similarly but with a change of incident particle being nonrelativistic, $v_\chi = 10^{-3}$, to ultrarelativistic, $v_\nu \to 1$. To leading order in the nonrelativistic expansion of the atomic current, the results for elastic scattering and discrete excitations by the ν_e-e interaction are

$$\left.\frac{d\sigma^{(nl)}}{dT}\right|_{\nu_e e} \approx \frac{G_F^2}{16\pi} m_H [(1 + 4\sin^2\theta_w)^2 + (-1)^2]$$

$$\times V_L R^{(nl)}\left(\kappa = \frac{\mu}{m_e} q\right), \tag{28}$$

with

$$V_L = \left(1 - \frac{T^2}{q^2}\right)^2 \left[\left(2 - \frac{T}{E_\nu}\right)^2 - \left(\frac{q}{E_\nu}\right)^2\right]. \tag{29}$$

If the processes go through the ν_e-p interaction, changes in Eq. (28) are the vector and axial coupling strengths and the momentum κ that fixes the response function $R^{(nl)}$. Notice that Eq. (28) differs from the DM scattering through the c_1-type interaction, i.e., Eq. (9), only in coupling strength, kinematic factor V_L, and lack of nonrelativistic enhancement factor $1/v_\chi^2$. Therefore, their dependences on T track with what are shown in the upper panels of Figs. 1 and 2, with a scale shift which can be fixed by setting $d\sigma^{(1s)}/dT|_{\nu_e p} \approx d\sigma^{(\nu_e p)}/dT \sim 1.5 \times 10^{-20}\,\text{mb}/\text{ev}$ at $T \to 0$. For most of the range of T, the nuclear contribution is dominant. For ionization by the ν_e-e interaction, a formula similar to Eq. (11) is obtained:

$$\frac{d\sigma^{(\text{ion})}}{dT}\bigg|_{\nu_e e} \approx \frac{G_F^2}{16\pi}[(1+4\sin^2\theta_w)^2 + (-1)^2]$$

$$\times \frac{E_\nu - T}{E_\nu} \int d\cos\theta V_L R^{(\text{ion})}\left(\kappa = \frac{\mu}{m_e}q\right). \quad (30)$$

Unlike Eq. (11), the integration over the scattering angle in Eq. (30) is weighed by V_L. Therefore, it is better to carry out explicit calculations to see how neutrinos ionize hydrogen atoms.

Figure 9 shows the numerical results of neutrino-hydrogen scattering for selected reaction channels with either the ν_e-e or ν_e-p interaction being turned on. The neutrino energy is fixed at $E_\nu = 300$ keV, which is at the peak of the pp neutrino spectrum. As previously anticipated, the energy dependences of elastic and discrete excitation channels track well with ones of DM scattering with c_1-type interactions (see the left panel of Fig. 3 for a one-to-one comparison) before the sharp edge which indicates that maximum energy $T_{\text{max}}^{(\nu)} = 2E_\nu^2/(2E_\nu + m_H) \sim 180$ eV that a 300-keV neutrino can transfer to a hydrogen atom with two-body final states. In elastic scattering, the nuclear contribution dominates; $d\sigma/dT$ is about 4.7×10^{-21} mb/eV, which is close to the free ν_e-p result and 12 orders of magnitude smaller than DM scattering with $c_1^{(p)} = 10^{-8}/\text{MeV}^2$. In the $1s$-to-$2s$ excitation, the electronic contribution dominates at the peak region with $d\sigma/dT$ at the order of 10^{-22}–10^{-23} mb/eV, which is about 10 to 11 orders of magnitude smaller than DM scattering with $c_1^{(e)} = 10^{-8}/\text{MeV}^2$. The ionization case is quite interesting for its different energy dependence due to the weighting of V_L: The electronic contribution not only dominates in the entire range of T considered (not like the

$E_\nu = 300$keV

FIG. 9. Comparison of ν_e cross sections with the electron (νe) and proton (νp) in a hydrogen atom for selected channels including (i) elastic ($1s$), (ii) discrete excitation to $2s$, and (iii) ionization (ion). Interference terms resulting from $\nu_e e$ and $\nu_e p$ amplitudes are ignored.

DM case, it is only true near threshold) but also its flat value at 7.2×10^{-24} mb/eV is close to the free ν_e-e result. Note that similar observations have been made, e.g., in Refs. [41,49], that when incident neutrino energy E_ν is much larger than T and atomic scales, the binding effect of atomic electrons can be safely ignored. Near ionization threshold, the DM scattering with $c_1^{(e)} = 10^{-8}/\text{MeV}^2$ is about 9 to 10 orders of magnitude bigger than the neutrino one.

In practical experiments, however, the actual count rates for DM and neutrino scattering events, which determine the physical reach of an experimental search for DM, should be convoluted with fluxes. We shall not try to fold detailed spectra of galactic DM and solar neutrino sources into this hydrogen case, but just roughly compare their fluxes: For DM, by using the galactic DM density $\rho_\chi \sim 0.3$ GeV/cm^2 and the averaged DM velocity $\bar{v}_\chi \sim 10^{-3}$, the flux is crudely estimated as $\rho_\chi \bar{v}_\chi/m_\chi$; for $m_\chi = 50$ MeV, it is $2 \times 10^8/\text{cm}^2$-s. For solar neutrino, the total flux is about $10^{11}/\text{cm}^2$-s. As it lies mostly in the energy range of a few hundred keV, almost the entire flux can effectively contribute to hydrogen discrete excitations and ionization. As a result, the 50 MeV DM flux is smaller than the solar neutrino flux by about 3 order of magnitudes, so such a LDM interaction can only be constrained in direct searches, if without special techniques to discriminate neutrino backgrounds, to the level that it is large enough to compensate for this relative suppression in flux. Note that the LDM interactions strengths we assume to make plots in Secs. III A and III B should produce count rates well above the neutrino backgrounds, so there is room for improvement.

D. Remarks on study beyond hydrogen

Detector response plays an important role in the interpretation of a DM scattering event at a direct detector. A reliable understanding requires three important ingredients: (1) the DM-matter interaction, (2) the differential cross section $d\sigma/dT$ for the primary scattering process, and (3) the following energy loss mechanism in detector media.

In this work, we address (1) following the bottom-up approach based on effective field theory. Its advantage is general; the scan of possible parameter space is only limited by available experiments and model independent. For (2), we consider the simplest hydrogen case, where the initial bound state and the final state, either unchanged, discretely excited, or ionized can all be solved analytically. For other complex atoms, extending our current work involves detailed, numerically intensive many-body physics so that all of the wave functions and scattering amplitudes of various EFT operators can be reliably calculated. As demonstrated by a series of recent works on neutrino-germanium scattering processes [49–51], we consider the prospect of properly addressing (1) and (2) for LDM
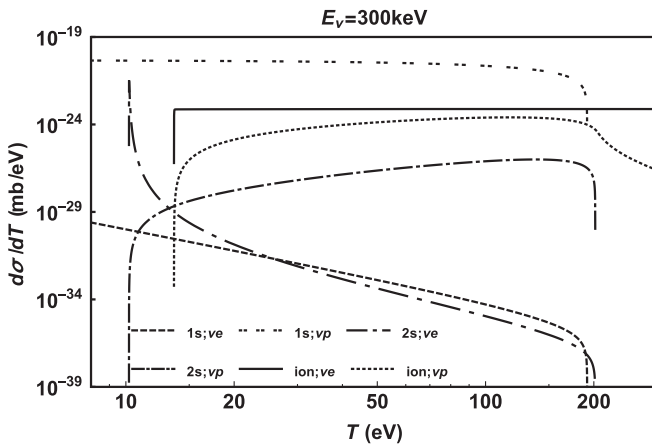
searches with germanium and xenon detectors very promising (similar to what has been done in Refs. [40,52,53] for the WIMP searches). We do not try to address (3) in this work for two reasons. First, there are semiempirical formulas, simulation packages, and experimental calibrations that can give reasonable descriptions. Second, a satisfactory account of them based on first principles needs many nontrivial microscopic inputs such as cross sections of atom-atom collisions, decay and recombination rates of atoms, ions, and molecular states, etc., and a statistical convolution of them—an interesting but also extremely challenging task.

Our theory approach laid down above for understanding the detector response in LDM searches differs from the one of Ref. [27], on which the first direct limit on sub-GeV LDM was derived using the XENON 10 data [28]. However, except the obvious choice of EFT vs model-specific DM-matter interactions, those differences in (2) and (3) will only be clearly demonstrated after we carry out the same calculation of LDM-xenon scattering, which is currently ongoing.

IV. SUMMARY

In this paper, we study the scattering processes of sub-GeV DM particles and hydrogen atoms, including elastic, atomic discrete excitation, and atomic ionization channels. The interactions of DM with electrons and nucleons are both included and formulated in a general framework based on nonrelativistic effective field theory. In addition to the leading-order spin-independent and spin-dependent contact terms, we also include the possibility of long-range DM interactions and a few next-to-leading-order terms. Some of the interaction terms yield orthogonal scattering amplitudes, but there are also interference terms. Disentanglement of various interaction terms can, in principle, be done by their different dependence on DM energy deposition in scattering cross sections.

On the assumption of the same dark matter coupling strengths, it is found that DM-electron interactions

dominate the inelastic transitions to discrete excited states and ionization continuum around their threshold regions (sizes of these regions depend on interaction types), and DM-nucleon interactions become more important with increasing energy and dominate in elastic scattering. These conclusions can be used to guide the searches of sub-GeV DM interactions in optimal experimental configurations and kinematics. For DM-electron interactions, the inelastic peaks of discrete excitations and ionizations in scattering cross sections, which can be taken as smoking-gun signals of DM scattering, can further increase an experiment's constraining power. For DM-nucleon interactions, although the elastic scattering is the best channel for light DM particles which cannot deposit observable energies in detectors, one has to rely on the high energy part of ionization processes.

The energy and momentum transfers involved in sub-GeV DM scattering overlap typical atomic scales, so studies of issues such as binding effects and electron/nuclear recoil mechanism, which play important roles in interpreting experimental data, require detailed many-body calculations. This case study of hydrogen, where both binding and recoil can be taken into account most simply, therefore provides a useful qualitative understanding of what is to be anticipated in sub-GeV DM scattering off practical detector materials such as germanium and xenon.

[1] K. Olive *et al.* (Particle Data Group), Chin. Phys. C **38**, 090001 (2014).

[2] R. Essig, J. A. Jaros, W. Wester, P. H. Adrian, S. Andreas *et al.*, arXiv:1311.0029.

[3] J. L. Feng and J. Kumar, Phys. Rev. Lett. **101**, 231301 (2008).

[4] J. L. Feng, M. Kaplinghat, H. Tu, and H.-B. Yu, J. Cosmol. Astropart. Phys. 07 (2009) 004.

[5] C. Boehm and P. Fayet, Nucl. Phys. **B683**, 219 (2004).

[6] C. Boehm, P. Fayet, and J. Silk, Phys. Rev. D **69**, 101302 (2004).

[7] N. Borodatchenkova, D. Choudhury, and M. Drees, Phys. Rev. Lett. **96**, 141802 (2006).

[8] M. Pospelov, A. Ritz, and M. B. Voloshin, Phys. Lett. B **662**, 53 (2008).

[9] P. Fayet, Phys. Rev. D **75**, 115017 (2007).

[10] D. Hooper and K. M. Zurek, Phys. Rev. D **77**, 087302 (2008).

[11] M. Pospelov, A. Ritz, and M. B. Voloshin, Phys. Rev. D **78**, 115012 (2008).

[12] K. Rajagopal, M. S. Turner, and F. Wilczek, Nucl. Phys. **B358**, 447 (1991).

[13] L. Covi, J. E. Kim, and L. Roszkowski, Phys. Rev. Lett. **82,** 4180 (1999).

[14] K.-Y. Choi, L. Covi, J. E. Kim, and L. Roszkowski, J. High Energy Phys. 04 (2012) 106.

[15] S. Dodelson and L. M. Widrow, Phys. Rev. Lett. **72,** 17 (1994).

[16] X.-D. Shi and G. M. Fuller, Phys. Rev. Lett. **82,** 2832 (1999).

[17] A. D. Dolgov and S. H. Hansen, Astropart. Phys. **16,** 339 (2002).

[18] A. Boyarsky, J. Lesgourgues, O. Ruchayskiy, and M. Viel, Phys. Rev. Lett. **102,** 201304 (2009).

[19] K. N. Abazajian, Phys. Rev. Lett. **112,** 161303 (2014).

[20] J. Knodlseder *et al.*, Astron. Astrophys. **441,** 513 (2005).

[21] G. Weidenspointner *et al.*, Nature (London) **451,** 159 (2008).

[22] N. Prantzos *et al.*, Rev. Mod. Phys. **83,** 1001 (2011).

[23] E. Bulbul, M. Markevitch, A. Foster, R. K. Smith, M. Loewenstein, and S. W. Randall, Astrophys. J. **789,** 13 (2014).

[24] A. Boyarsky, O. Ruchayskiy, D. Iakubovskyi, and J. Franse, Phys. Rev. Lett. **113,** 251301 (2014).

[25] D. Hooper and L. Goodenough, Phys. Lett. B **697,** 412 (2011).

[26] D. Hooper and T. Linden, Phys. Rev. D **84,** 123005 (2011).

[27] R. Essig, J. Mardon, and T. Volansky, Phys. Rev. D **85,** 076007 (2012).

[28] R. Essig, A. Manalaysay, J. Mardon, P. Sorensen, and T. Volansky, Phys. Rev. Lett. **109,** 021301 (2012).

[29] H. An, M. Pospelov, J. Pradler, and A. Ritz, Phys. Lett. B **747,** 331 (2015).

[30] R. Bernabei *et al.* (DAMA Collaboration), Eur. Phys. J. C **56,** 333 (2008).

[31] R. Bernabei *et al.* (DAMA and LIBRA Collaborations), Eur. Phys. J. C **67,** 39 (2010).

[32] R. Bernabei *et al.*, Eur. Phys. J. C **73,** 2648 (2013).

[33] R. Bernabei, P. Belli, F. Montecchia, F. Nozzoli, F. Cappella *et al.*, Phys. Rev. D **77,** 023506 (2008).

[34] J. Kopp, V. Niro, T. Schwetz, and J. Zupan, Phys. Rev. D **80,** 083502 (2009).

[35] R. Foot, Phys. Rev. D **90,** 121302 (2014).

[36] R. Essig, E. Kuflik, S. D. McDermott, T. Volansky, and K. M. Zurek, J. High Energy Phys. 11 (2013) 193.

[37] R. Essig, J. Mardon, M. Papucci, T. Volansky, and Y.-M. Zhong, J. High Energy Phys. 11 (2013) 167.

[38] B. Batell, R. Essig, and Z. Surujon, Phys. Rev. Lett. **113,** 171802 (2014).

[39] J. Fan, M. Reece, and L.-T. Wang, J. Cosmol. Astropart. Phys. 11 (2010) 042.

[40] A. L. Fitzpatrick, W. Haxton, E. Katz, N. Lubbers, and Y. Xu, J. Cosmol. Astropart. Phys. 02 (2013) 004.

[41] J.-W. Chen, C.-P. Liu, C.-F. Liu, and C.-L. Wu, Phys. Rev. D **88,** 033006 (2013).

[42] A. Nordsieck, Phys. Rev. **93,** 785 (1954).

[43] A. R. Holt, J. Phys. B **2,** 1209 (1969).

[44] D. Belkić, J. Phys. B **14,** 1907 (1981).

[45] M. S. Gravielle and J. E. Miraglia, Comput. Phys. Commun. **69,** 53 (1992).

[46] P. Vogel and J. Engel, Phys. Rev. D **39,** 3378 (1989).

[47] E. Fischbach, J. T. Grunewald, S. P. Rosen, H. Spivack, and B. Kayser, Phys. Rev. D **15,** 97 (1977).

[48] J. F. Beacom, W. M. Farr, and P. Vogel, Phys. Rev. D **66,** 033001 (2002).

[49] J.-W. Chen, H.-C. Chi, K.-N. Huang, C.-P. Liu, H.-T. Shiao, L. Singh, H. T. Wong, C.-L. Wu, and C.-P. Wu, Phys. Lett. B **731,** 159 (2014).

[50] J.-W. Chen, H.-C. Chi, H.-B. Li, C.-P. Liu, L. Singh, H. T. Wong, C.-L. Wu, and C.-P. Wu, Phys. Rev. D **90,** 011301(R) (2014).

[51] J.-W. Chen, H.-C. Chi, K.-N. Huang, H.-B. Li, C.-P. Liu, L. Singh, H. T. Wong, C.-L. Wu, and C.-P. Wu, Phys. Rev. D **91,** 013005 (2015).

[52] A. L. Fitzpatrick, W. Haxton, E. Katz, N. Lubbers, and Y. Xu, arXiv:1211.2818.

[53] N. Anand, A. L. Fitzpatrick, and W. C. Haxton, Phys. Rev. C **89,** 065501 (2014).